

CONFIDENTIAL

Copy 4  
RM L57D09

NACA RM L57D09

FOR REFERENCE  
NOT TO BE TAKEN FROM



# RESEARCH MEMORANDUM

INVESTIGATION OF THE LOW-SPEED STABILITY AND CONTROL  
CHARACTERISTICS OF A 1/7-SCALE MODEL OF THE  
NORTH AMERICAN X-15 AIRPLANE

By Peter C. Boisseau

Langley Aeronautical Laboratory  
Langley Field, Va.

LIBRARY COPY

JUN 27 1957

LANGLEY AERONAUTICAL LABORATORY  
LIBRARY, NACA  
LANGLEY FIELD, VIRGINIA

CLASSIFICATION CHANGED

to UNCLASSIFIED

By authority of TPA#33 CLASSIFIED DOCUMENT 10-28-60

This material contains information affecting the National Defense of the United States within the meaning of the espionage laws, Title 18, U.S.C., Secs. 793 and 794, the transmission or revelation of which in any manner to an unauthorized person is prohibited by law.

## NATIONAL ADVISORY COMMITTEE FOR AERONAUTICS

WASHINGTON

June 25, 1957

CONFIDENTIAL

UNCLASSIFIED



3 1176 01437 9086

NATIONAL ADVISORY COMMITTEE FOR AERONAUTICS

## RESEARCH MEMORANDUM

INVESTIGATION OF THE LOW-SPEED STABILITY AND CONTROL  
CHARACTERISTICS OF A 1/7-SCALE MODEL OF THE  
NORTH AMERICAN X-15 AIRPLANE

By Peter C. Boisseau

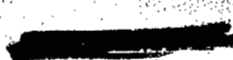
## SUMMARY

An investigation of the low-speed power-on stability and control characteristics of a 1/7-scale free-flying model of the North American X-15 airplane has been made by the Langley Free-Flight Tunnel Section. The model was flown over an angle-of-attack range from  $8^\circ$  to  $30^\circ$ , and only relatively low-altitude conditions were simulated.

Although the longitudinal stability was low, it was considered to be satisfactory up to an angle of attack of about  $30^\circ$  where the model experienced a pitch-up. The pitch-up was mild and could be prevented by proper use of longitudinal control. The lateral stability characteristics were satisfactory at angles of attack up to about  $30^\circ$  where static directional instability caused the model to be directionally divergent. The Dutch roll oscillation was heavily damped. The differentially deflected horizontal tail provided very good roll control over the angle-of-attack range tested ( $8^\circ$  to  $30^\circ$ ), and effectiveness was maintained up to the angle of attack at which the model diverged. The large favorable yawing moments produced at low and moderate angles of attack by the tail roll control did not have any unfavorable effects on the flight characteristics of the model. Differential deflection of the horizontal tail had little effect on the longitudinal flight characteristics.

## INTRODUCTION

An investigation has been made of the low-speed power-on stability and control characteristics of a 1/7-scale free-flying model representing configuration number 1 of the North American X-15 airplane. (Configuration number 1 was the original arrangement in which the major portion



of the vertical-tail area was on top of the fuselage.) The primary purpose of this investigation was to aid in the evaluation of one of the unique features of the airplane - the use of the horizontal tail for roll control. This type of roll control has appeared to be very promising on the basis of various force-test investigations (refs. 1 to 9). One of the questions that has arisen regarding the use of such a control is the effect of its large favorable yawing moments on dynamic lateral control characteristics. In this model flight investigation, therefore, the lateral control characteristics of the X-15 configuration were studied with particular attention being given to the effect of the large favorable yawing moments.

The investigation included flight tests in the Langley full-scale tunnel to determine the low-speed flight characteristics of the model over an angle-of-attack range from  $8^\circ$  to  $30^\circ$  and force tests in the Langley free-flight tunnel to determine the static and dynamic stability and control characteristics over an angle-of-attack range from  $0^\circ$  to  $40^\circ$ . The investigation also included force tests of the model with symmetrical upper and lower vertical tails, but no flight tests were made with this configuration.

In order to permit a better interpretation of the free-flight tests in terms of the full-scale airplane, a comparison was made between the results of the force tests of the flight-test model at a low Reynolds number ( $0.59 \times 10^6$ ) in the free-flight tunnel and unpublished data obtained at a higher Reynolds number ( $1.30 \times 10^6$ ).

#### SYMBOLS

The longitudinal data are referred to the stability system of axes and the lateral data are referred to the body system of axes. (See fig. 1.) The origin of the axes was located to correspond to a center-of-gravity position of 25.0 percent of the mean aerodynamic chord for the model in both the clean and the landing configurations.

S	wing area, sq ft
$\bar{c}$	wing mean aerodynamic chord, ft
V	airspeed, ft/sec
b	wing span, ft
q	dynamic pressure, $\frac{\rho V^2}{2}$ , lb/sq ft

$\rho$	air density, slugs/cu ft
$\beta$	angle of sideslip, deg
$\psi$	angle of yaw, deg
$\phi$	angle of bank, deg
$\alpha$	angle of attack of fuselage reference line, deg
$k$	reduced-frequency parameter, $\frac{\omega b}{2V}$
$\omega$	angular velocity, radians/sec
$\eta$	angle of attack of principal longitudinal axis of airplane; positive when principal axis is above flight path at nose, deg
$X_S$	longitudinal force, lb
$Y$	lateral force, lb
$Z_S$	normal force, lb
$F_L$	lift force, lb
$F_D$	drag force, lb
$F_Y$	side force, lb
$M_Y$	pitching moment, ft-lb
$M_X$	rolling moment, ft-lb
$M_Z$	yawing moment, ft-lb
$C_L$	lift coefficient, Lift/qS
$C_D$	drag coefficient, Drag/qS
$C_m$	pitching-moment coefficient, $\frac{M_Y}{qS\bar{c}}$

$C_n$  yawing-moment coefficient,  $\frac{M_z}{qSb}$

$C_l$  rolling-moment coefficient,  $\frac{M_x}{qSb}$

$C_Y$  lateral-force coefficient,  $\frac{F_Y}{qS}$

$\Delta C_Y, \Delta C_n, \Delta C_l$  incremental force and moments due to a control deflection

$$C_{Y\beta} = \frac{\partial C_Y}{\partial \beta} \text{ per degree}$$

$$C_{n\beta} = \frac{\partial C_n}{\partial \beta} \text{ per degree}$$

$$C_{l\beta} = \frac{\partial C_l}{\partial \beta} \text{ per degree}$$

$\delta_t$  deflection of horizontal tail when used for longitudinal control, deg

$\delta_h$  differential deflection of horizontal-tail surfaces when used as roll control, positive when left-hand control has more positive deflection, deg

$\delta_r$  deflection of all-moving vertical tail (upper part only), deg

$\delta_f$  flap deflection measured perpendicular to hinge line, deg

$$C_{Y\delta_h} = \frac{\Delta C_Y}{\delta_h} \text{ per degree}$$

$$C_{n\delta_h} = \frac{\Delta C_n}{\delta_h} \text{ per degree}$$

$$C_{l\delta_h} = \frac{\Delta C_l}{\delta_h} \text{ per degree}$$

$$C_{Y\delta_r} = \frac{\Delta C_Y}{\delta_r} \text{ per degree}$$

$$C_{n\delta_r} = \frac{\Delta C_n}{\delta_r} \text{ per degree}$$

$$C_{l\delta_r} = \frac{\Delta C_l}{\delta_r} \text{ per degree}$$

Subscript:

s            stability axis

## APPARATUS AND TESTS

### Model

The 1/7-scale model used in the investigation was constructed at the Langley Laboratory. A three-view drawing of the model is shown in figure 2, and a photograph of the model is shown in figure 3. Table I gives the mass and dimensional characteristics of the full-scale design and the scaled-up mass and dimensional characteristics of the model.

Because of an error in construction that was not discovered until after completion of the test program, the horizontal-tail span of the model was actually about 3.5 percent greater than it should have been. (See table I.) Since the force-test data obtained with this tail were in reasonably good agreement with higher Reynolds number data for a model with the correct size tail, it was not felt to be necessary to rerun the present program with the correct size tail.

For the flight tests, thrust was provided by compressed air supplied through flexible hoses to two nozzles at the rear of the fuselage. The amount of thrust in the model could be varied and the maximum output per nozzle was about 10 to 12 pounds. The controls were operated remotely by the pilots by means of flicker-type (full on or off) pneumatic servomechanisms which were actuated by electric solenoids. The all-movable horizontal tail could also be trimmed in flight. The control deflections used in the flight tests were  $\delta_h = \pm 9^\circ$ ,  $\delta_r = \pm 4.5^\circ$ , and  $\delta_t = \pm 8.5^\circ$ .

### Test Equipment and Setup

The flight investigation was conducted in the test section of the Langley full-scale tunnel with the test setup illustrated in figure 4. In this setup there is an overhead safety cable to prevent the model from

crashing. Combined with this cable is another cable composed of plastic hoses which provide the compressed air for thrust and wires which provide power for the control actuators. These cables are attached to the model at about the center-of-gravity location. The thrust controller varies the thrust of the model by remotely controlling the air flow to the model through a valve located at the top of the entrance cone. The thrust controller and the pitch pilot must coordinate their efforts in order to maintain steady flight. Another operator adjusts the safety cable so as to keep it slack during flight and takes up the slack to prevent the model from crashing if it goes out of control. A second pilot who controls the rolling and yawing motions of the model is located near the bottom of the exit cone. Motion-picture records of the flights are obtained with cameras located at the side of the test section and at the top and the bottom of the exit cone.

The flight-test technique employed with this setup will be explained by describing a typical flight. A flight was started with the model being towed from the safety cable which was attached for towing purposes at a point about 1 foot forward of the center of gravity of the model. When the tunnel speed reached the flying speed of the model, the model thrust was increased until the flight cable became slack, at which time the safety cable was released from its forward attachment point on the fuselage. Adjustments to the horizontal tail and thrust were then made, if necessary, to trim the model for the particular airspeed. The flight was then continued to higher or lower airspeeds by changing the trim setting of the horizontal tail and making the necessary adjustments to tunnel speed and model thrust to maintain steady flight.

## DETERMINATION OF STATIC STABILITY AND CONTROL CHARACTERISTICS OF FLIGHT-TEST MODEL

### Longitudinal Stability and Control Characteristics

Force tests were made to determine the static longitudinal stability and control characteristics of the model in the clean and landing configurations for an angle-of-attack range of  $0^\circ$  to  $40^\circ$ . These tests were made with horizontal tail off and for horizontal-tail incidences of  $0^\circ$  and  $-5^\circ$ . Tests were also made with the horizontal tail differentially deflected  $\pm 5^\circ$ . All the force tests were conducted at a dynamic pressure of 4.69 pounds per square foot, which corresponds to an airspeed of about 63 feet per second at the standard sea-level conditions and to a test Reynolds number of  $0.59 \times 10^6$  based on the mean aerodynamic chord of 1.47 feet.

The static longitudinal stability characteristics of the free-flight model are compared with unpublished data for higher Reynolds numbers in figure 5 for the clean configuration with the horizontal tail off and on.

Unpublished data are presented for the model with fuselage fairings off and on and for the free-flight model with fairings on. In general, the characteristics of the two models are similar. With horizontal tail on, both models are longitudinally stable at angles of attack up to about  $30^\circ$  and then become unstable. This instability is caused by a loss in horizontal-tail effectiveness as indicated by comparing the pitching-moment increment between the curves for the model with tail off and tail on.

It is interesting to note the lift characteristics of the model, which are quite unusual because of the large fairings. The lift curve for the wing-body combination (fairing off) breaks at a fairly low angle of attack where the wing stalls. The addition of the fairing delays the break to a much higher angle of attack and nearly doubles the maximum lift coefficient. The addition of the horizontal tail causes a further increase in the maximum lift and delays the stall so that the lift of the complete model is still increasing at  $40^\circ$  angle of attack. (See fig. 5.)

Presented in figure 6 are the static longitudinal stability and control characteristics of the free-flight-tunnel model in the clean and landing conditions for tail incidences of  $0^\circ$  and  $-5^\circ$ . A comparison of the data shows that deflecting the flap increased the stability at high angles of attack but reduced the tail effectiveness over the angle-of-attack range. The reduction in tail effectiveness is believed to be associated with a decrease in dynamic pressure in the region of the horizontal tail as a result of deflecting the flap and also to partial stalling of the surfaces resulting from the increased downwash at a given angle of attack with the flaps deflected.

The effects on the longitudinal characteristics of tail incidence and differential deflection of the horizontal tail are shown in figures 7 and 8 for the model in the clean and landing configurations, respectively. Differential deflection of the horizontal tail generally had little effect on the longitudinal characteristics.

#### Lateral Stability and Control Characteristics

Force tests were made to determine the static lateral stability and control characteristics of the model in both the clean and the landing conditions over a sideslip range from  $20^\circ$  to  $-20^\circ$  for angles of attack from  $0^\circ$  to  $36^\circ$ . These tests were for the complete model and for the model with the upper vertical tail off. Some tests were also made over a sideslip range of  $10^\circ$  to  $-10^\circ$  with upper and lower vertical tails off and for a symmetrical vertical-tail arrangement. These data were obtained at the same dynamic pressure as the longitudinal stability and control data.

The lateral stability characteristics are presented in figures 9 and 10 for the model in the clean and landing configurations, respectively. The data of figures 9 and 10 are summarized in figure 11 in terms of the side-force parameter  $C_{Y\beta}$ , the directional-stability parameter  $C_{n\beta}$ , and the effective-dihedral parameter  $-C_{l\beta}$ . The directional stability of the model in the clean configuration was approximately constant at angles of attack up to about  $16^\circ$  and then dropped rapidly to negative values at an angle of attack of about  $30^\circ$ . This can be attributed both to an increase in the unstable moment of the wing-fuselage combination and to a decrease in the contribution of the upper vertical tail to the directional stability. The directional stability of the model in the landing configuration was about the same as that for the clean condition at angles of attack up to  $20^\circ$  but it became negative at a lower angle of attack. The positive effective dihedral of the model in the clean configuration increased up to moderate angles of attack and then decreased to zero at about the same angle of attack at which  $C_{n\beta}$  became zero. Deflecting the flap increased the value of  $-C_{l\beta}$  at low angles of attack but decreased the values at high angles of attack and resulted in the effective dihedral becoming zero at a lower angle of attack.

Presented in figure 12 are the variations of the lateral stability parameters  $C_{Y\beta}$ ,  $C_{n\beta}$ , and  $-C_{l\beta}$  with angle of attack for the free-flight model in the clean configuration with all vertical tails off and on. These data are compared with unpublished data for higher Reynolds numbers. The data show that the higher Reynolds number model had somewhat more directional stability than the free-flight model in the low and moderate angle-of-attack range, but both models become directionally unstable at about the same angle of attack ( $30^\circ$ ). The value of the effective dihedral parameter  $-C_{l\beta}$  was somewhat greater for the higher Reynolds number model over the angle-of-attack range.

The effect of various vertical-tail configurations on the lateral stability parameters is shown in figure 13. The model with the symmetrical vertical-tail configuration is shown to have much less directional stability than configuration number 1, particularly at high angles of attack, and it becomes directionally unstable at  $28^\circ$ . With the drop portion of the lower vertical tail off, the model suffers a considerable loss in directional stability over the entire angle-of-attack range and becomes unstable at an angle of attack of  $25^\circ$ . The upper vertical tail of configuration number 1 produces an appreciable value of  $-C_{l\beta}$  over the low and moderate angle-of-attack range.

Presented in figures 14 and 15 are the variations of  $C_{l\delta_h}$ ,  $C_{n\delta_h}$ , and  $C_{y\delta_h}$  produced by deflecting the horizontal tail differentially  $\pm 5^\circ$  for mean tail incidences of  $0^\circ$  and  $-5^\circ$  for the model in the clean and landing configurations with the vertical tail off and on. For the model in the clean condition (fig. 14) the roll effectiveness for tail incidences of  $0^\circ$  and  $-5^\circ$  is similar up to moderately high angles of attack where the effectiveness for  $0^\circ$  incidence drops off more rapidly, apparently because one surface is stalling. For the model in the landing configuration (fig. 15), overall variation of roll effectiveness with angle of attack was generally similar to that for the clean condition but the values of  $C_{l\delta_h}$  were somewhat smaller. This reduction in roll effectiveness with flap deflection, like the reduction in tail pitching effectiveness previously mentioned, is attributed to a decrease in dynamic pressure at the tail and to partial stalling of the tail surfaces.

The data show that large positive yawing moments were obtained with the vertical tail either off or on at low moderate angles of attack. These large yawing moments result in large values of the parameter  $\frac{C_{n\delta_h}}{C_{l\delta_h}}$  which are usually considered undesirable from a flying-qualities standpoint. As the angle of attack increased, the favorable yaw decreased and finally became unfavorable at high angles of attack.

The major portion of the large yawing moment at low angles of attack results from the fact that the horizontal tail has  $15^\circ$  negative dihedral, so that when the tail is deflected differentially a rather large side force (and, hence, a yawing moment) is produced. In other airplane configurations in which the horizontal tail has been used for roll control, most of the favorable yawing moment has been produced by loads induced on the vertical tail by the horizontal tail, but for the X-15 configuration this effect was small because of the particular tail arrangement.

The rudder is effective over the whole angle-of-attack range as shown in figure 16. The rudder also produces sizable adverse rolling moments, especially at the higher angles of attack.

#### Damping in Roll and Yaw

Rotary oscillation tests were made to determine the rolling and yawing derivatives of the free-flight model in the clean configuration with upper vertical tail off and on. The tests were made for a range

of values of the reduced-frequency parameter  $k$ . All rotary tests were made at a dynamic pressure of 5.06 pounds per square foot which corresponds to an airspeed of approximately 65 feet per second at standard sea-level conditions and to an effective Reynolds number of  $0.60 \times 10^6$  based on the mean aerodynamic chord of 1.47 feet.

The variations of the rolling derivative  $(C_{l_p} + C_{l_{\dot{\beta}}} \sin \alpha)$  and the yawing derivative  $(C_{n_r} + C_{n_{\dot{\beta}}} \cos \alpha)$  with angle of attack are shown in figure 17 for two values of the reduced-frequency parameter  $k$  (0.06 and 0.16). The data show that the values of damping in roll and yaw are essentially constant up to an angle of attack of about  $20^\circ$  and then the values of both derivatives increase with increasing angle of attack. At the lower angles of attack there is very little effect of frequency, but at the higher angles more damping is obtained with the lower frequency.

#### FLIGHT TESTS

Flight tests were made to study the stability and control characteristics of the model over an angle-of-attack range from  $8^\circ$  to  $30^\circ$ . The lower angle-of-attack limit was determined by the highest speed at which the model could be conveniently flown. The model was flown with coordinated roll and rudder control, with roll control alone, and with rudder-alone control. Roll control deflections of  $\pm 9^\circ$  and a rudder deflection of  $\pm 4.5^\circ$  were used for all flight conditions. The model was flown only with the configuration number 1 vertical tail. Only relatively low-altitude conditions were simulated.

The model behavior during flight was observed by the pitch pilot located at the side of the test section and by the roll-and-yaw pilot located in the rear of the test section. The results obtained were based on pilots' observations and data obtained from motion-picture records.

#### FLIGHT-TEST RESULTS AND DISCUSSION

A motion-picture film supplement covering flight tests of a model similar to the X-15 airplane has been prepared and is available on loan. A request card form and a description of the film will be found at the back of this paper, on the page immediately preceding the abstract and index page.

## Interpretation of Flight-Test Results

The mass data presented in table I show that the model had values of the scaled-up moments of inertia generally similar to those of the airplane. It has been shown that the static stability characteristics of the low Reynolds number, free-flight model are in good agreement with the unpublished higher Reynolds number results. It is likely, however, that the changes noted in the stability parameters at high angles of attack will occur at somewhat higher angles of attack for the airplane than for the model. The dynamic behavior of the airplane is therefore expected to be similar to that of the free-flight model except that corresponding dynamic behavior might occur at higher angles of attack.

In interpreting the lateral-control characteristics of models in terms of full-scale airplanes, it has been found necessary in some cases to consider the differences in piloting technique used on the models and the airplanes. Studies have shown that airplanes which have high yawing inertia and low rolling inertia, such as the present model, tend to execute a pure rolling motion about the principal longitudinal axis of inertia, at least during the early stages of a rolling maneuver. When these airplanes roll in this manner, an adverse sideslip angle about the stability axis is produced which is approximately equal to the angle of inclination of the principal axis times the sine of the angle of bank ( $\eta \sin \phi$ ). For instance, for a given angle of inclination of the principal axis of  $20^\circ$ , an airplane of this type when banked  $30^\circ$  will have an angle of adverse sideslip of  $10^\circ$  about the stability axis. Since the pilot of a free-flight model flies the model from a remote position and can perform only very limited maneuvers, he does not object to the model's executing essentially pure roll about the principal axis and apparently cannot detect the resulting adverse sideslip about the stability axis that might be objectionable to the pilot of the full-scale airplane. The estimation of the adverse sideslip characteristics of the airplane based on the model flight tests is therefore expected to be optimistic.

## Longitudinal Stability and Control

The longitudinal stability was considered to be low for the angle-of-attack range tested, but the model could be flown satisfactorily in either the clean or the landing configuration. At an angle of attack of about  $30^\circ$  there was a definite pitch-up tendency which resulted in the model reaching very high angles of attack when no control was applied to prevent it. The pilot could usually prevent a pitch-up by proper use of control, however, since the pitching motion was fairly slow and the longitudinal control was powerful. Differential deflection of the horizontal tail for lateral control did not appear to affect the

longitudinal characteristics of the model. These flight characteristics are generally what would be expected on the basis of the static data shown in figures 6 and 7.

### Lateral Stability

The lateral stability characteristics were found to be generally satisfactory up to the maximum angle of attack at which the model could be flown ( $\alpha = 30^\circ$ ). The lateral (Dutch roll) oscillation was very well damped for all flight conditions tested. In fact, the damping of the oscillation following a disturbance was so heavy that it appeared to be almost deadbeat. This heavy damping can be attributed in part to the large values of the damping-in-roll and yaw derivatives shown in figure 17.

As the model approached an angle of attack of  $30^\circ$  there was an increasing tendency for the model to diverge in sideslip, but the pilot was able to maintain flight by paying careful attention to control. When the angle of attack reached  $30^\circ$ , the model became more and more difficult to control and eventually experienced a directional divergence. The reason for this behavior can be explained by the static directional stability data of figures 9 to 11. As the angle of attack increases the directional stability decreases and the sideslip range over which the model is directionally stable also decreases. (See fig. 9(b).) At an angle of attack of about  $30^\circ$  the model becomes directionally unstable. Another factor which might have contributed to the directional divergence is the decrease in positive effective dihedral at the higher angles of attack.

### Lateral Control

The differentially deflected horizontal tail provided very good roll control over the entire angle-of-attack range tested ( $8^\circ$  to  $30^\circ$ ) and effectiveness was maintained up to the angle of attack at which the model diverged. The large favorable yawing moments shown in figures 13 and 14 did not produce any undesirable yawing motions. Satisfactory control was obtained with rudder except in the very highest angle-of-attack range. In the high angle-of-attack range it was necessary to coordinate the rudder with the roll control because of the greatly reduced yawing moments of the roll control at these angles of attack. (See fig. 13.)

It should be pointed out that the yawing-moment parameter  $\frac{C_{n\delta_h}}{C_{l\delta_h}}$  is only one of several factors that affect the yawing motions during

rolling maneuvers. For example, at moderate and high angles of attack, large adverse yawing moments might be produced by the yawing moment due to rolling velocity  $C_{n_p}$  and by the product-of-inertia effect. Thus

the resultant yawing moment might actually be small or adverse even

when the value of  $\frac{C_{n\delta_h}}{C_{l\delta_h}}$  is highly positive as shown by figure 14. It

would be expected that the most critical condition for excessive favorable yawing moments would be the low angle-of-attack range. At the lowest angle of attack reached in the model flight tests ( $8^\circ$ ), no objectionable yawing motions were produced by the roll control. At angles of attack lower than  $8^\circ$  the values of  $C_{n_p}$  and product-of-inertia

effect are likely to be quite small so that the resulting yawing moment

would approximately correspond to the values of  $\frac{C_{n\delta_h}}{C_{l\delta_h}}$  shown by figure 14. In this event the large favorable yawing moment might well

prove to be objectionable.

A few flights were made with only the rudder used for lateral control. Although the model experienced excessive sideslipping and was difficult to control, successful flights were made up to the angle of attack at which the model diverged.

#### CONCLUSIONS

Results have been presented from a free-flight stability and control investigation of a 1/7-scale model of the North American X-15 airplane. The model was flown over an angle-of-attack range from  $8^\circ$  to  $30^\circ$  and only relative low-altitude conditions were simulated. From the results, the following conclusions were drawn:

1. Although the longitudinal stability was low, it was considered to be satisfactory up to an angle of attack of about  $30^\circ$  where the model experienced a pitch-up. The pitch-up was mild and could be controlled.

2. The lateral stability characteristics were satisfactory up to an angle of attack of about  $30^\circ$  where static directional instability caused the model to be directionally divergent. The Dutch roll oscillation was heavily damped.

3. The differentially deflected horizontal tail provided very good roll control over the angle-of-attack range tested ( $8^{\circ}$  to  $30^{\circ}$ ) and effectiveness was maintained up to the angle of attack at which the model diverged. The large favorable yawing moments produced at low and moderate angles of attack by the tail roll control did not have any unfavorable effects on the flight characteristics of the model.

4. Differential deflection of the horizontal tail had little effect on the longitudinal flight characteristics.

Langley Aeronautical Laboratory,  
National Advisory Committee for Aeronautics,  
Langley Field, Va., March 22, 1957.

## REFERENCES

1. Koenig, David G.: Tests in the Ames 40- by 80-Foot Wind Tunnel of an Airplane Configuration With an Aspect Ratio 3 Triangular Wing and an All-Movable Horizontal Tail - Longitudinal and Lateral Characteristics. NACA RM A52L15, 1953.
2. Tinling, Bruce E., and Karpen, A. V.: The Effects of Trailing-Edge Flaps on the Subsonic Aerodynamic Characteristics of an Airplane Model Having a Triangular Wing of Aspect Ratio 3. NACA RM A54L07, 1955.
3. English, Roland D.: Free-Flight Investigation, Including Some Effects Of Wing Aeroelasticity, of the Rolling Effectiveness of an All-Movable Horizontal Tail With Differential Incidence at Mach Numbers From 0.6 to 1.5. NACA RM L54K30, 1955.
4. Critzos, Chris C.: Lateral-Control Investigation at Transonic Speeds of Differentially Deflected Horizontal-Tail Surfaces for a Configuration Having a 6-Percent-Thick  $45^\circ$  Sweptback Wing. NACA RM L55I26, 1955.
5. Savage, Howard F., and Tinling, Bruce E.: The Static Lateral and Directional Subsonic Aerodynamic Characteristics of an Airplane Model Having a Triangular Wing of Aspect Ratio 3. NACA RM A55B11, 1955.
6. Campbell, John P.: The Use of the Horizontal Tail for Roll Control. NACA RM L55L16a, 1956.
7. Mitchell, Jesse L., and Vitale, A. James: Free-Flight Investigation of the Control Effectiveness of a Differentially Deflected Horizontal Tail at Mach Numbers From 0.8 to 1.6. NACA RM L56B20, 1956.
8. Boisseau, Peter C.: Low-Speed Roll Effectiveness of a Differentially Deflected Horizontal-Tail Surface on a  $42^\circ$  Swept-Wing Model. NACA RM L56E03, 1956.
9. Spearman, M. Leroy: Limited Investigation of Effects of Differential Horizontal-Tail Deflection on Lateral Control Characteristics of Two Swept-Wing Airplane Models at Mach Numbers From 1.4 to 2.0. NACA RM L56I20, 1956.

TABLE I.- DIMENSIONAL AND MASS CHARACTERISTICS OF THE NORTH AMERICAN X-15 AIRPLANE  
AND SCALED-UP CHARACTERISTICS OF THE 1/7-SCALE MODEL TESTED IN THE  
LANGLEY FREE-FLIGHT TUNNEL

	Scaled-up model values	North American full scale
Weight, lb . . . . .	12,570	12,570
Wing loading, W/S, lb/sq ft . . . . .	62.85	62.85
Moments of inertia:		
$I_x$ , slug-ft <sup>2</sup> . . . . .	3,380	5,020
$I_y$ , slug-ft <sup>2</sup> . . . . .	60,800	65,100
$I_z$ , slug-ft <sup>2</sup> . . . . .	66,300	67,200
Relative density factor, $\mu_b$ . . . . .		35.83
Wing:		
Airfoil section . . . . .	NACA 66-005 (modified)	
Area, sq ft . . . . .		200
Span, ft . . . . .		22.35
Aspect ratio . . . . .		2.50
Root chord, ft . . . . .		14.91
Tip chord, ft . . . . .		2.98
Mean aerodynamic chord $\bar{c}$ , ft . . . . .		10.28
Longitudinal distance from leading edge at root chord to leading edge of $\bar{c}$ , ft . . . . .		3.29
Sweepback of leading edge, deg . . . . .		36.75
Sweepforward of trailing edge, deg . . . . .		17.75
Dihedral, deg . . . . .		0
Incidence, deg . . . . .		0
Flaps:		
Total area (behind hinge line), sq ft . . . . .		15.66
Span, ft . . . . .		16.32
Root chord, ft . . . . .		2.44
Tip chord, ft . . . . .		1.04
	Scaled-up model values	North American full scale
Horizontal tail:		
Airfoil section . . . . .	NACA 66-005 (modified)	NACA 66-005 (modified)
Area:		
Total, sq ft . . . . .	114.86	110.70
Exposed, sq ft . . . . .	54.76	50.60
Span:		
Total, ft . . . . .	18.24	17.65
Exposed, ft . . . . .	11.82	10.53
Root chord (on fuselage reference line), ft . . . . .	10.00	10.00
Tip chord, ft . . . . .	2.14	2.14
Sweepback of leading edge, deg . . . . .	49.62	50.54
Sweepback of trailing edge, deg . . . . .	18.30	19.28
Dihedral, deg . . . . .	-15.0	-15.0
Aspect ratio (based on total tail area) . . . . .	2.89	2.82
Longitudinal distance from 0.25 $\bar{c}$ to quarter chord of tail, ft . . . . .	8.92	8.92
Vertical tail (configuration number 1):		
Upper:		
Airfoil section . . . . .	10° double wedge (modified)	
Area (exposed), sq ft . . . . .		37.70
Span (exposed), ft . . . . .		6.89
Aspect ratio . . . . .		1.26
Lower:		
Airfoil section . . . . .	15° double wedge (modified)	
Area (exposed), sq ft . . . . .		13.68
Span (exposed), ft . . . . .		2.00
Aspect ratio . . . . .		0.29
Symmetrical tail:		
Upper:		
Airfoil section . . . . .	10° double wedge (modified)	
Area (exposed - each), sq ft . . . . .		39.59
Span (each), ft . . . . .		4.17
Aspect ratio (each) . . . . .		0.44
Lower (drop portion on):		
Airfoil section . . . . .	10° double wedge (modified)	
Area (exposed), sq ft . . . . .		38.17
Span, ft . . . . .		4.17
Aspect ratio . . . . .		0.46
Lower (drop portion off):		
Airfoil section . . . . .	10° double wedge (modified)	
Area (exposed), sq ft . . . . .		25.67
Span, ft . . . . .		2.50
Aspect ratio . . . . .		0.26

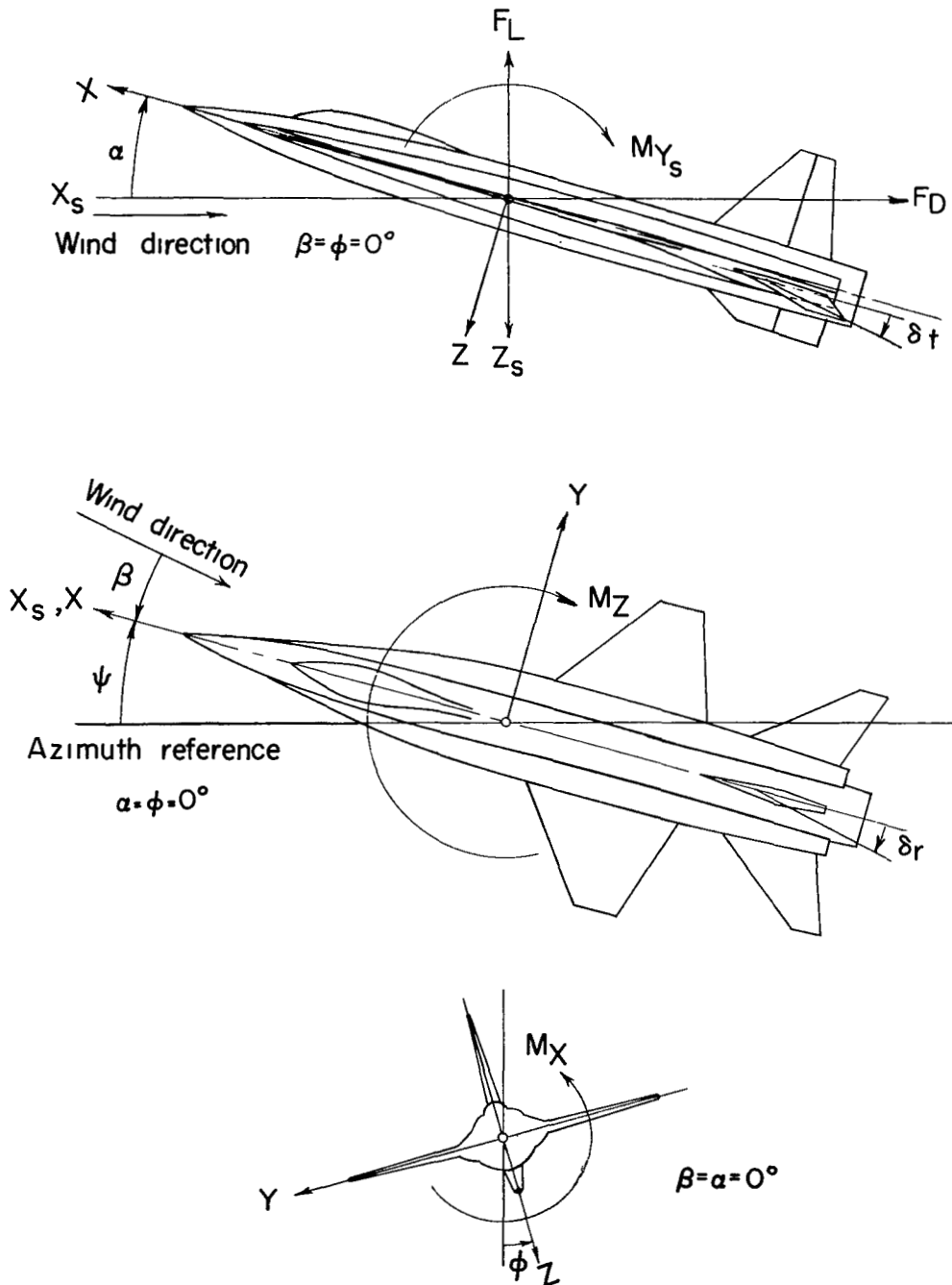


Figure 1.- System of axes used in investigation. Longitudinal data are referred to stability system of axes, and lateral data are referred to body system of axes. Arrows indicate positive directions of moments, forces, and angles.

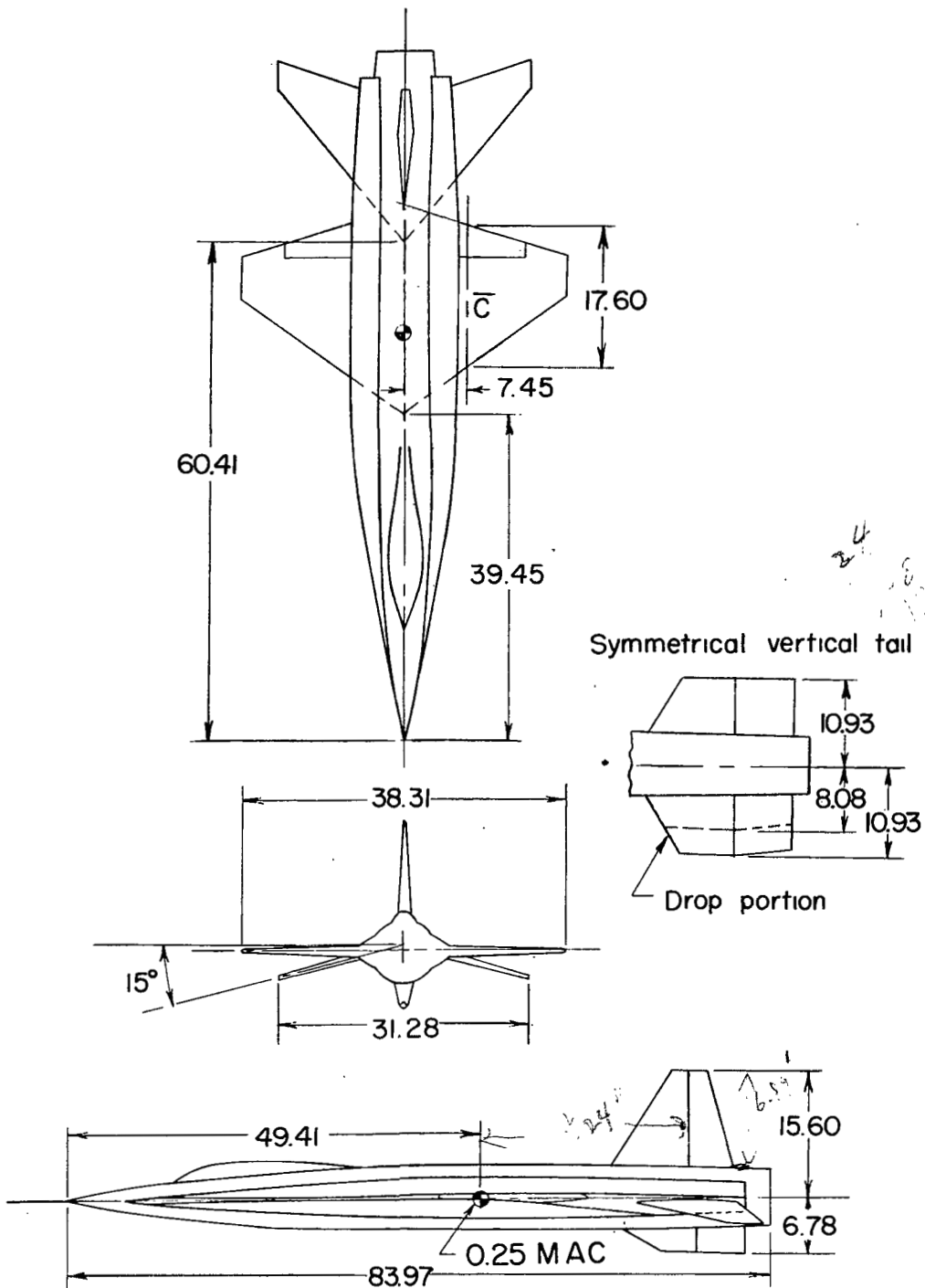


Figure 2.- Three-view drawing of 1/7-scale model of North American X-15 airplane used in investigation. All dimensions are in inches.

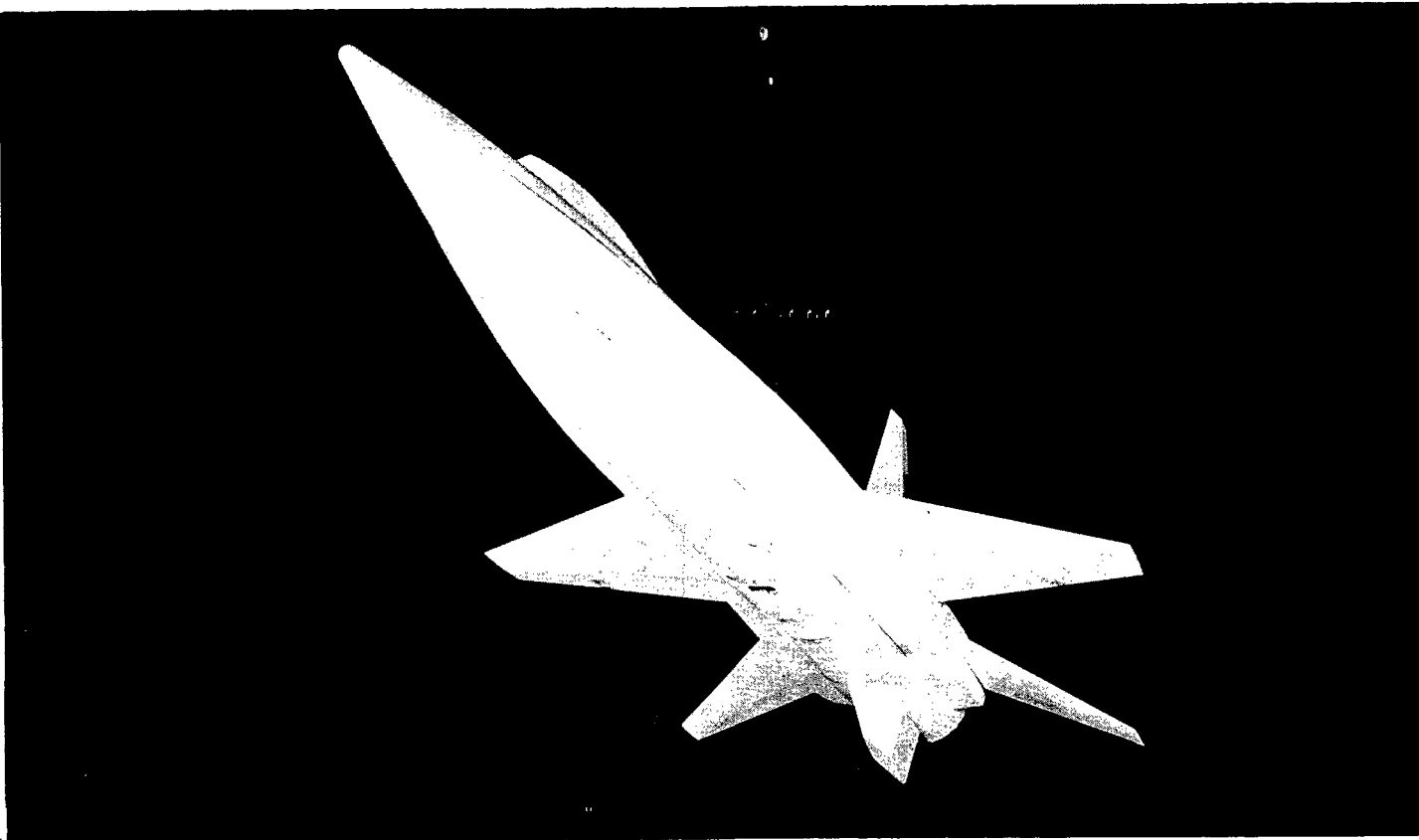


Figure 3.- Photograph of model used in investigation.

L-95227

PLN  
L-95227

1957  
1958  
1959  
1960  
1961  
1962  
1963  
1964  
1965  
1966  
1967  
1968  
1969  
1970  
1971  
1972  
1973  
1974  
1975  
1976  
1977  
1978  
1979  
1980  
1981  
1982  
1983  
1984  
1985  
1986  
1987  
1988  
1989  
1990  
1991  
1992  
1993  
1994  
1995  
1996  
1997  
1998  
1999  
2000

# FLIGHT-TEST SETUP

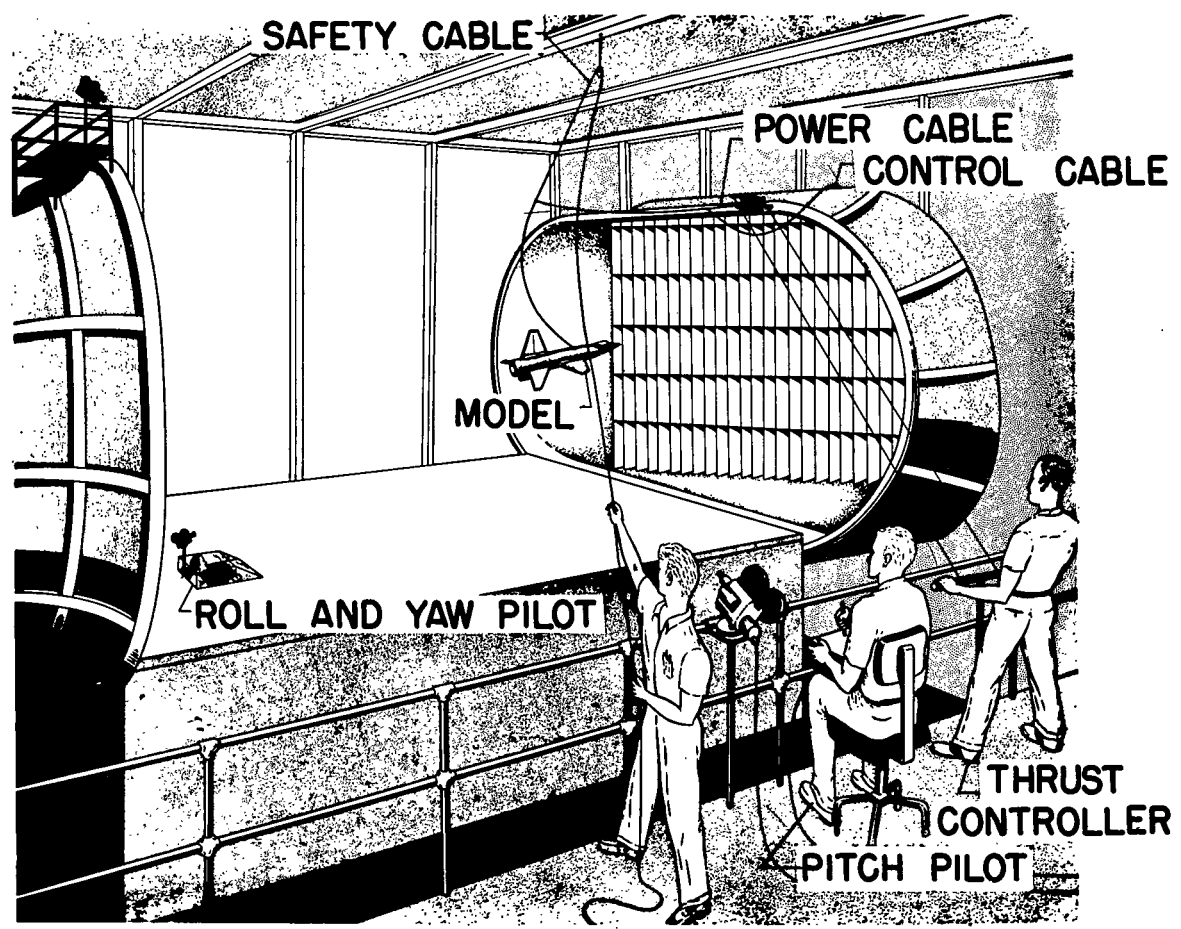


Figure 4.- Sketch of test setup in Langley full-scale tunnel.

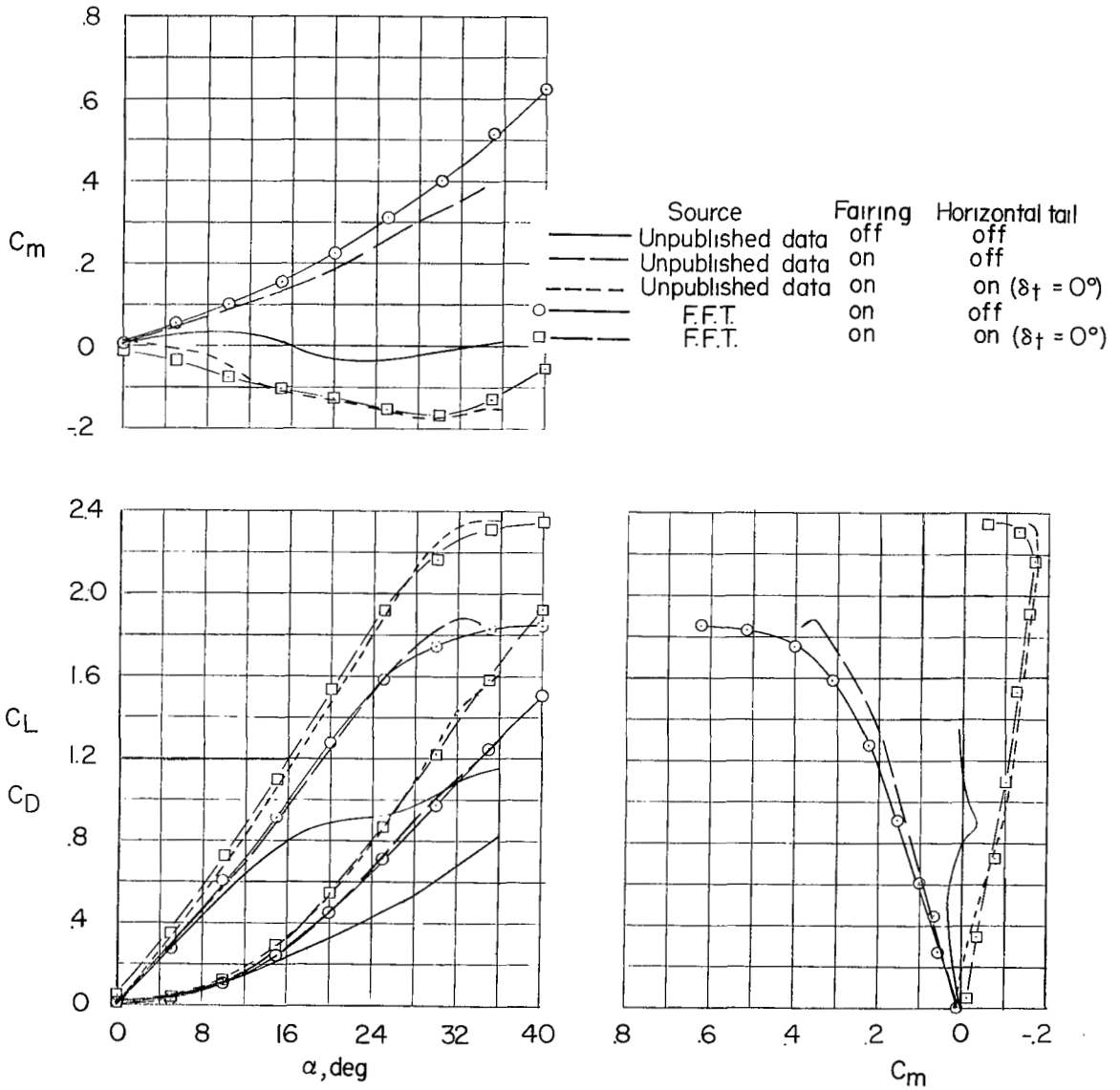


Figure 5.- Aerodynamic characteristics of model of X-15 airplane tested in Langley free-flight tunnel compared with unpublished data obtained at higher Reynolds numbers. Center of gravity at 0.25 mean aerodynamic chord;  $\delta_f = 0^\circ$ ;  $\beta = 0^\circ$ .

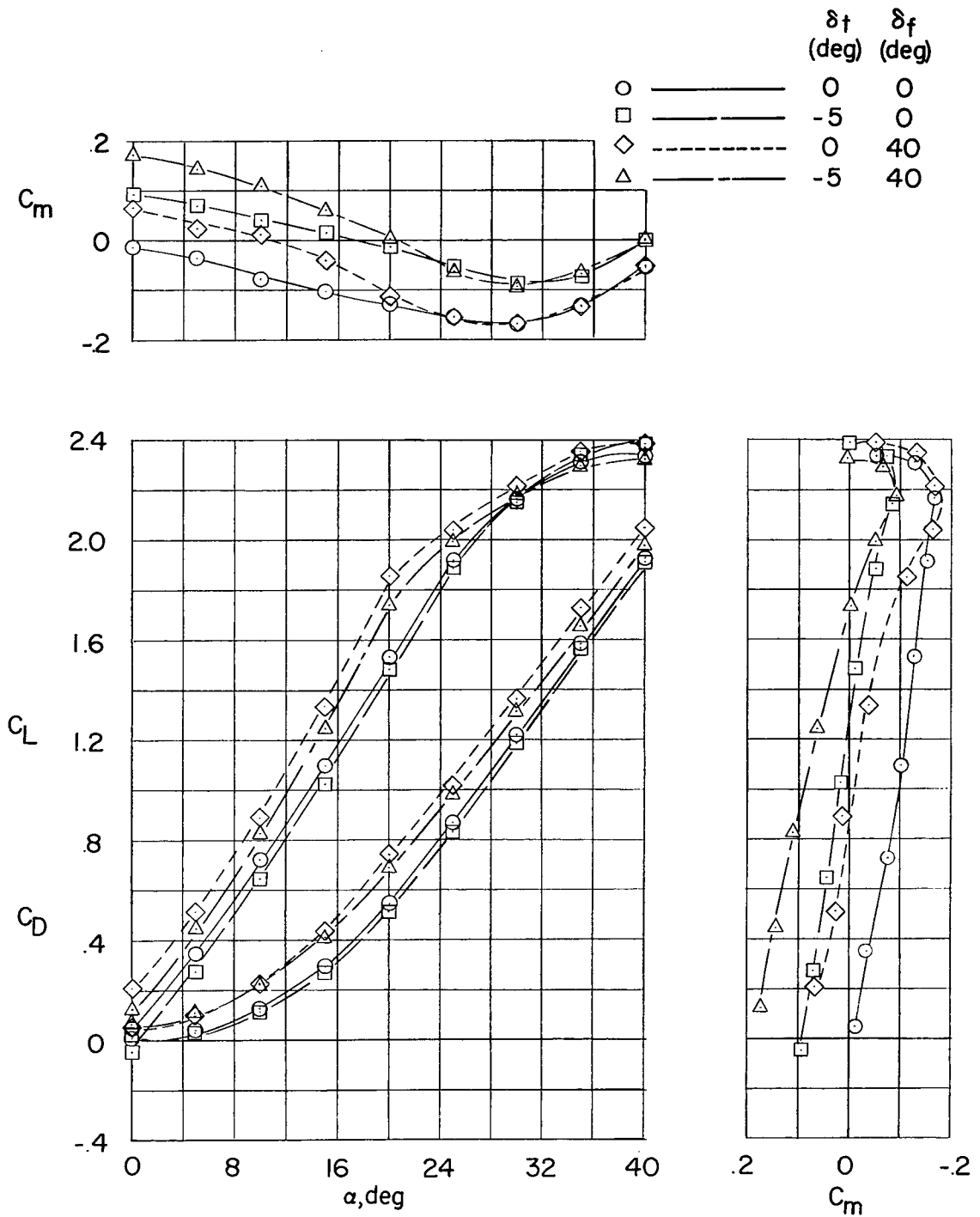


Figure 6.- Longitudinal characteristics of model in clean and landing configurations.  $\beta = 0^\circ$ .

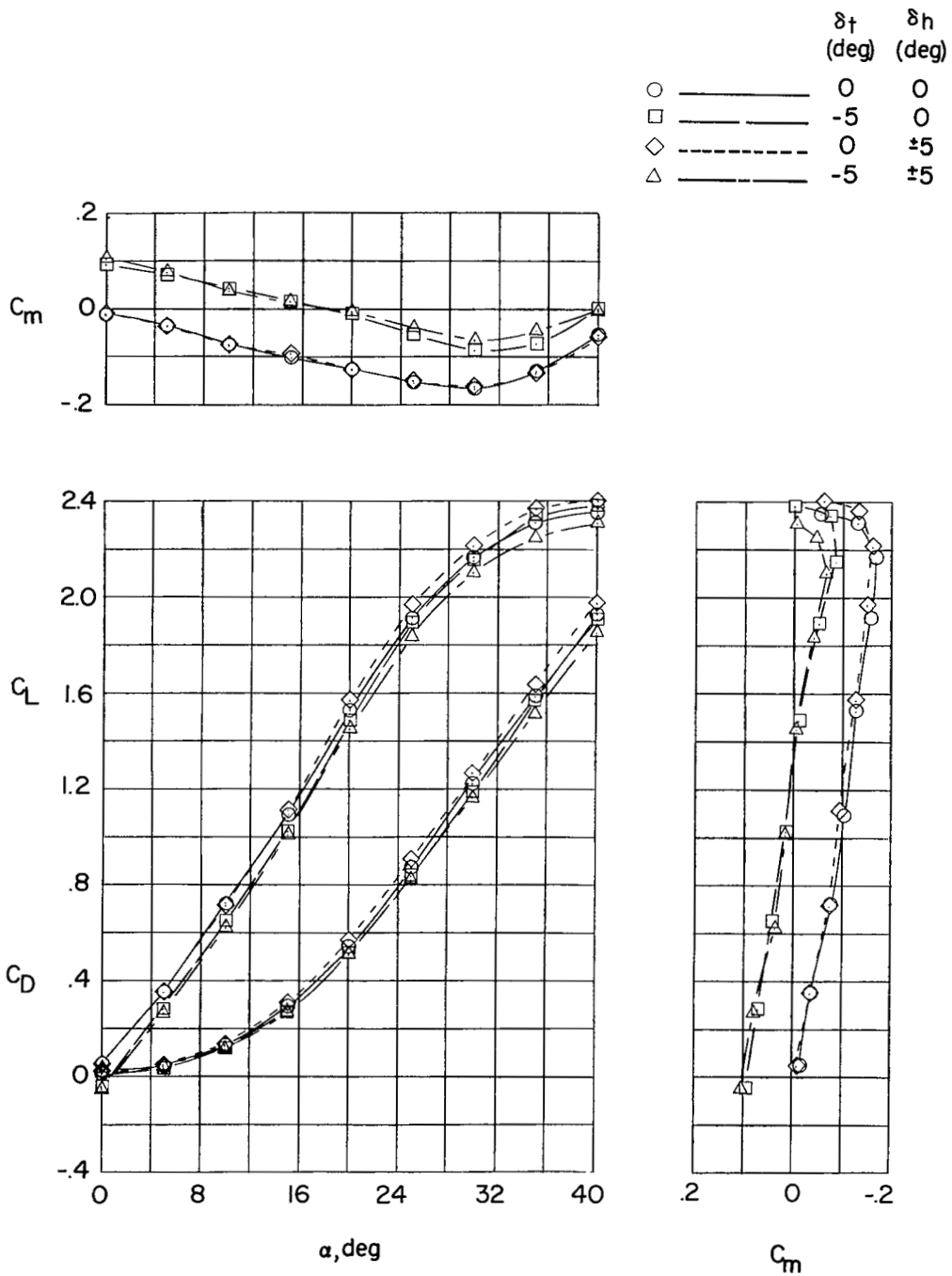


Figure 7.- Effect of differential deflection of horizontal tail on longitudinal characteristics of model in clean configuration.  $\delta_f = 0^\circ$ ;  $\beta = 0^\circ$ .

	$\delta_t$ (deg)	$\delta_h$ (deg)
○ —————	0	0
□ —————	-5	0
◇ - - - - -	0	±5
△ - - - - -	-5	±5

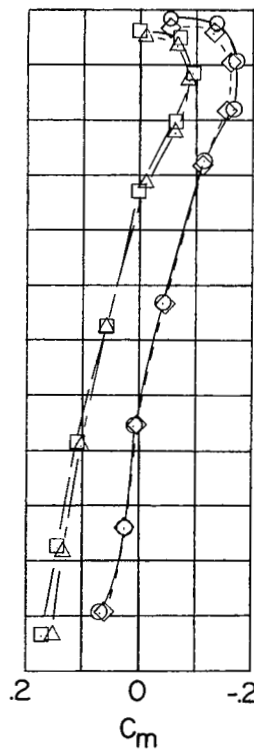
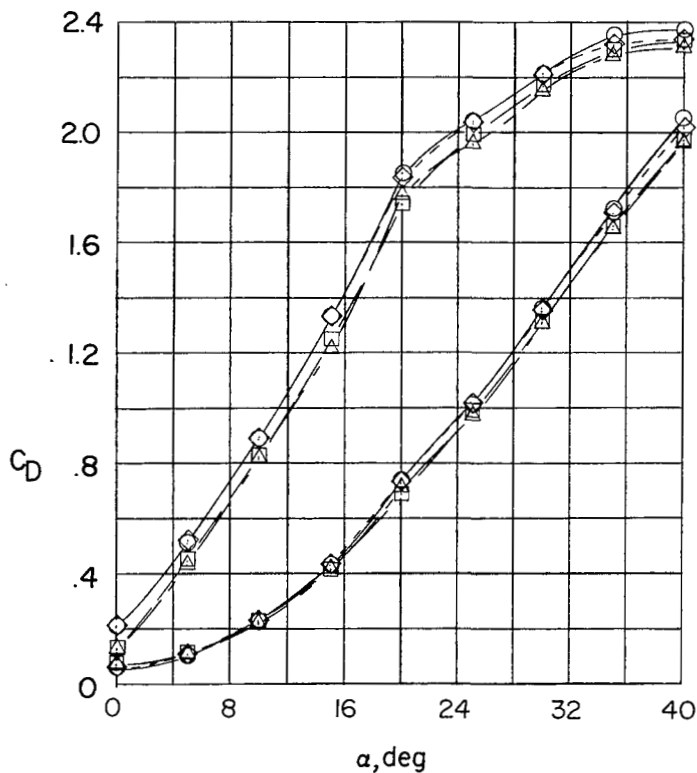
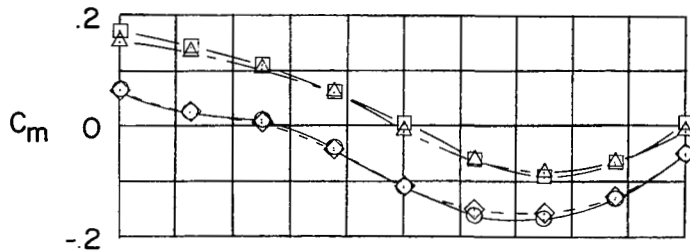
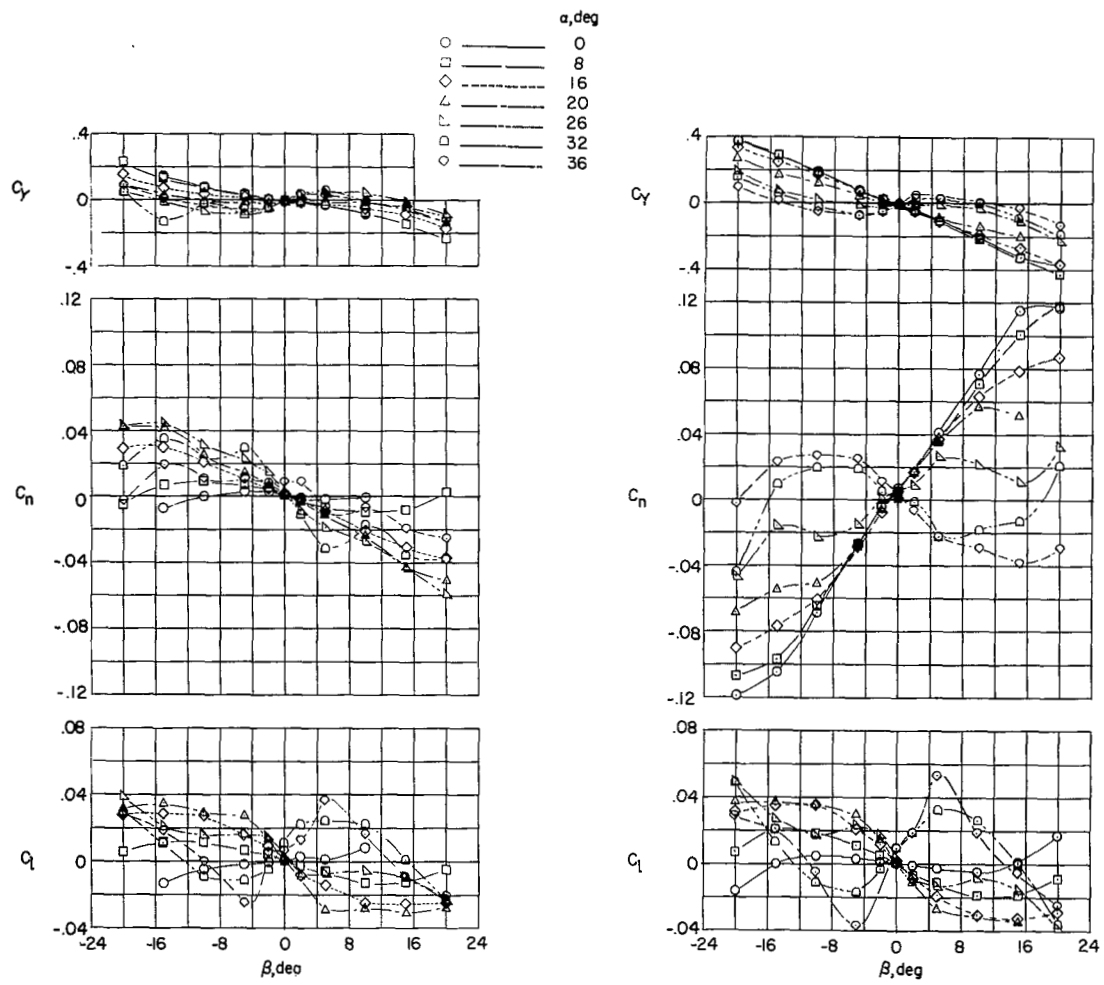


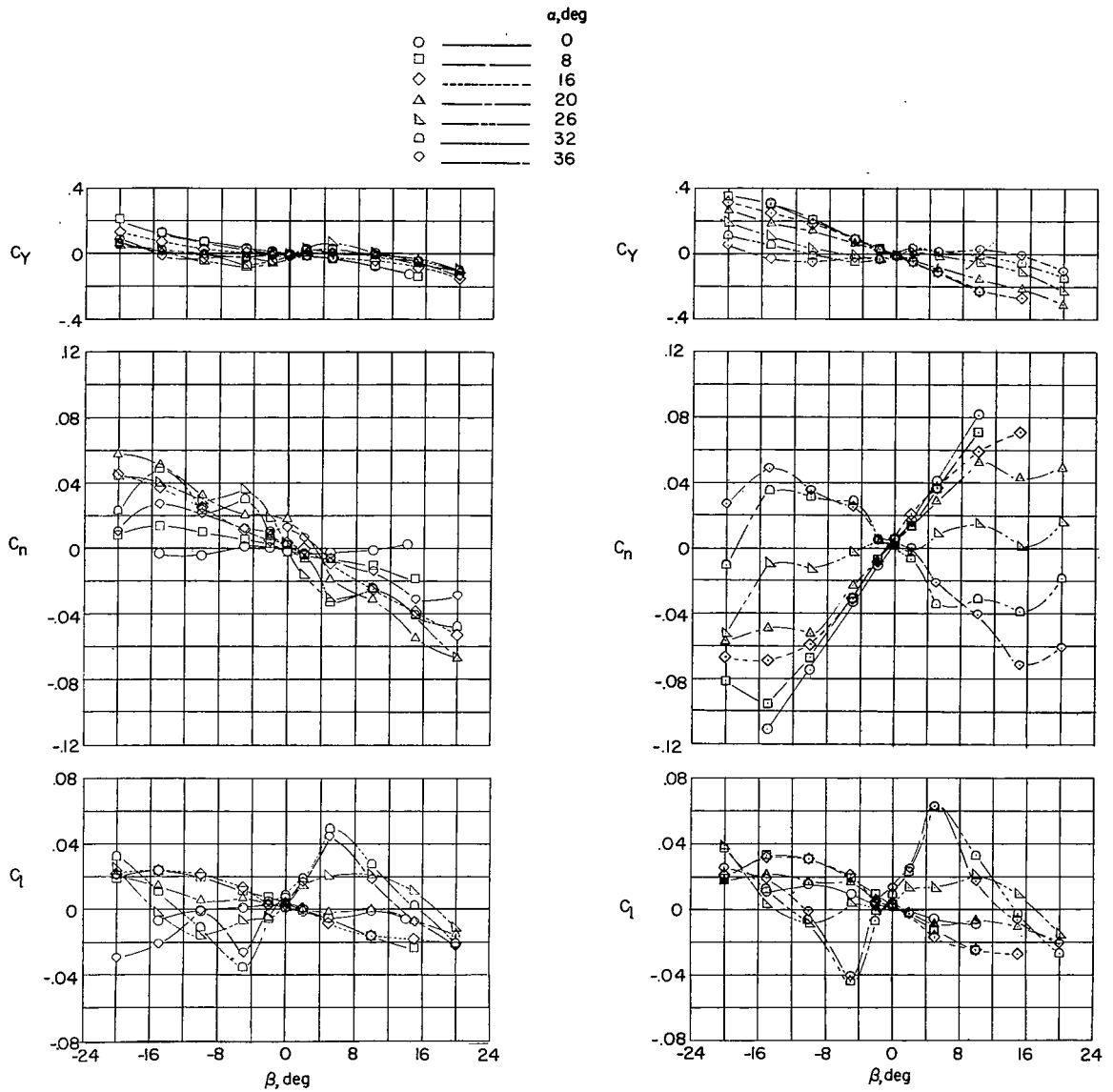
Figure 8.- Effect of differential deflection of horizontal tail on longitudinal characteristics of model in landing configuration.  $\delta_f = 40^\circ$ ;  $\beta = 0^\circ$ .



(a) Upper vertical tail off.

(b) Complete model.

Figure 9.- Variation of static lateral stability characteristics with angle of sideslip. Clean configuration;  $\delta_f = 0^\circ$ ;  $\delta_t = 0^\circ$ .



(a) Upper vertical tail off.

(b) Complete model.

Figure 10.- Variation of static lateral stability characteristics with angle of sideslip. Landing configuration;  $\delta_f = 40^\circ$ ;  $\delta_t = 0^\circ$ .

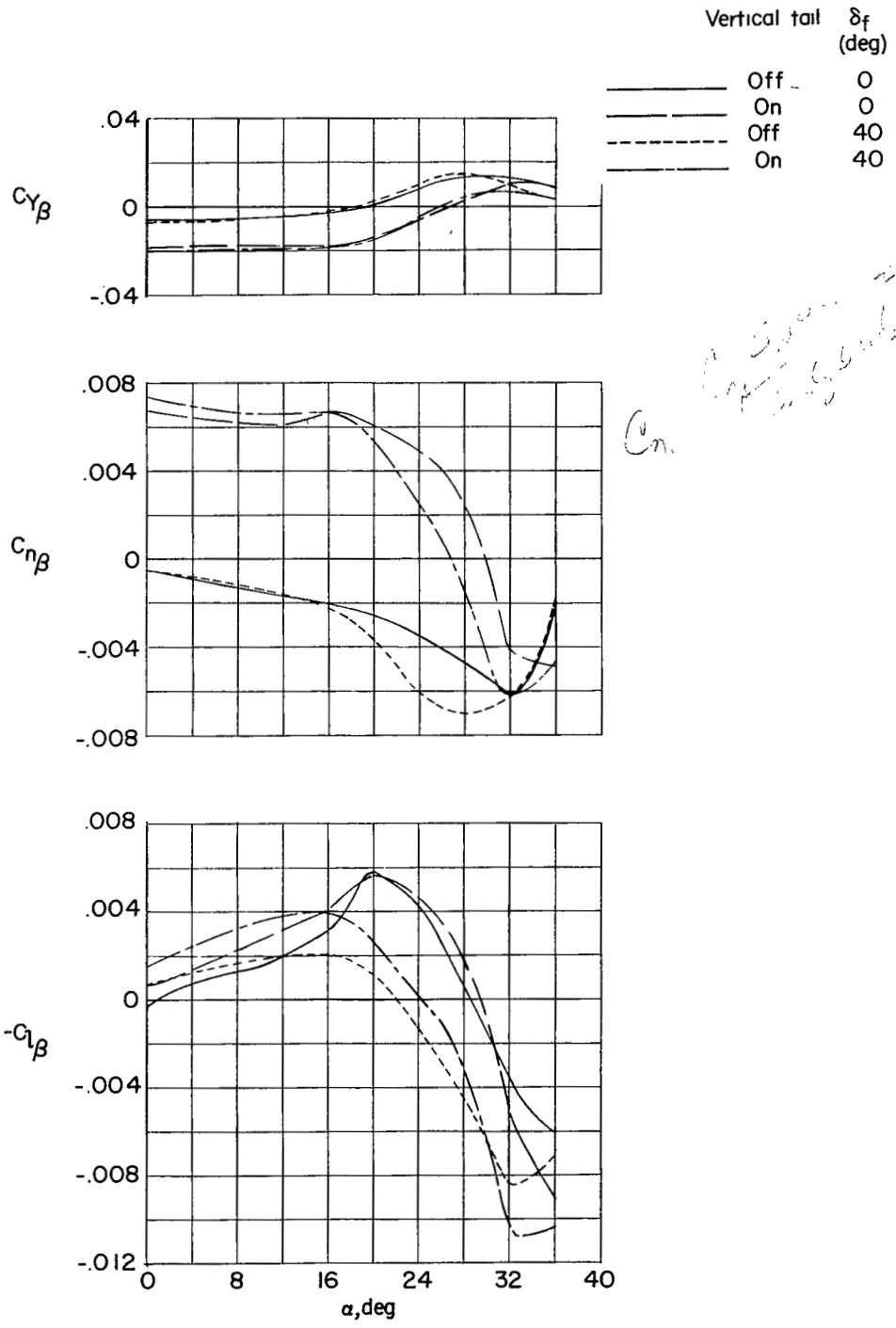


Figure 11.- Variation of static sideslip derivatives with angle of attack. Configuration number 1;  $\beta = \pm 5^\circ$ ;  $\delta_t = 0^\circ$ ;  $\delta_f = 0^\circ$ .

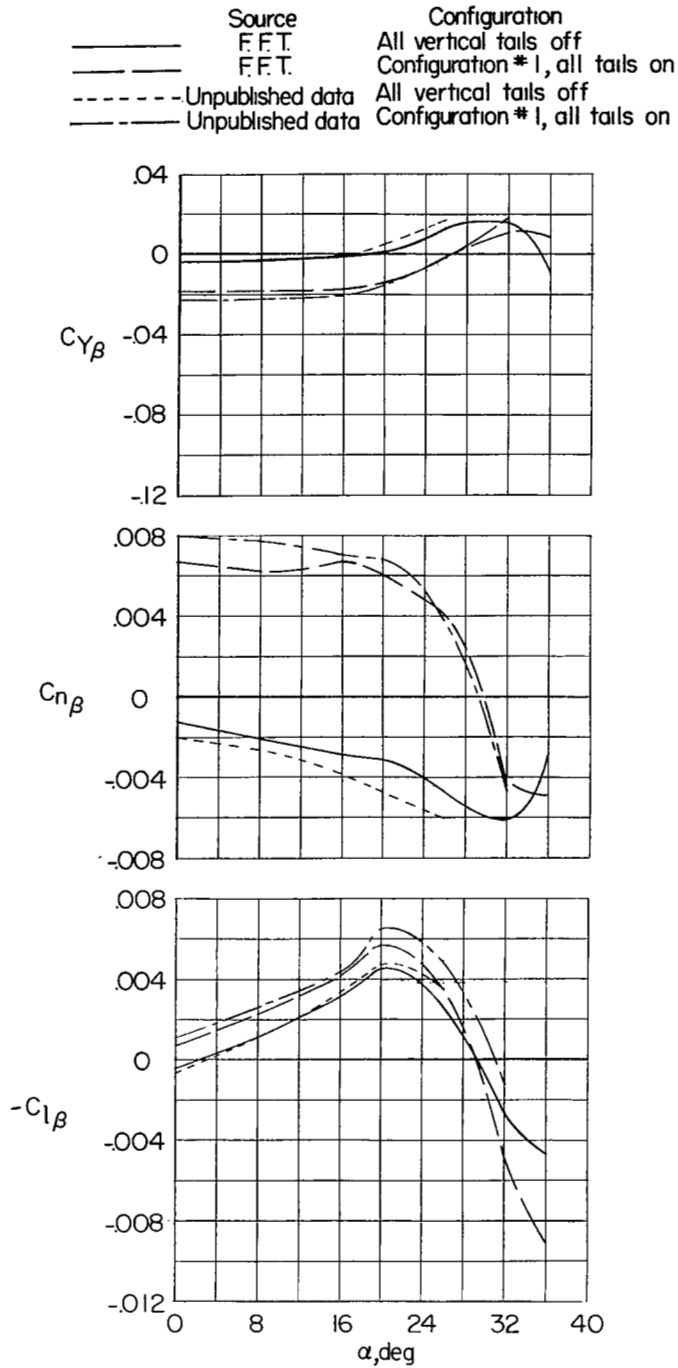


Figure 12.- Comparison of static sideslip derivatives of free-flight-tunnel model with unpublished data obtained at higher Reynolds numbers.  $\beta = \pm 5^\circ$ ;  $\delta_t = 0^\circ$ ;  $\delta_f = 0^\circ$ .

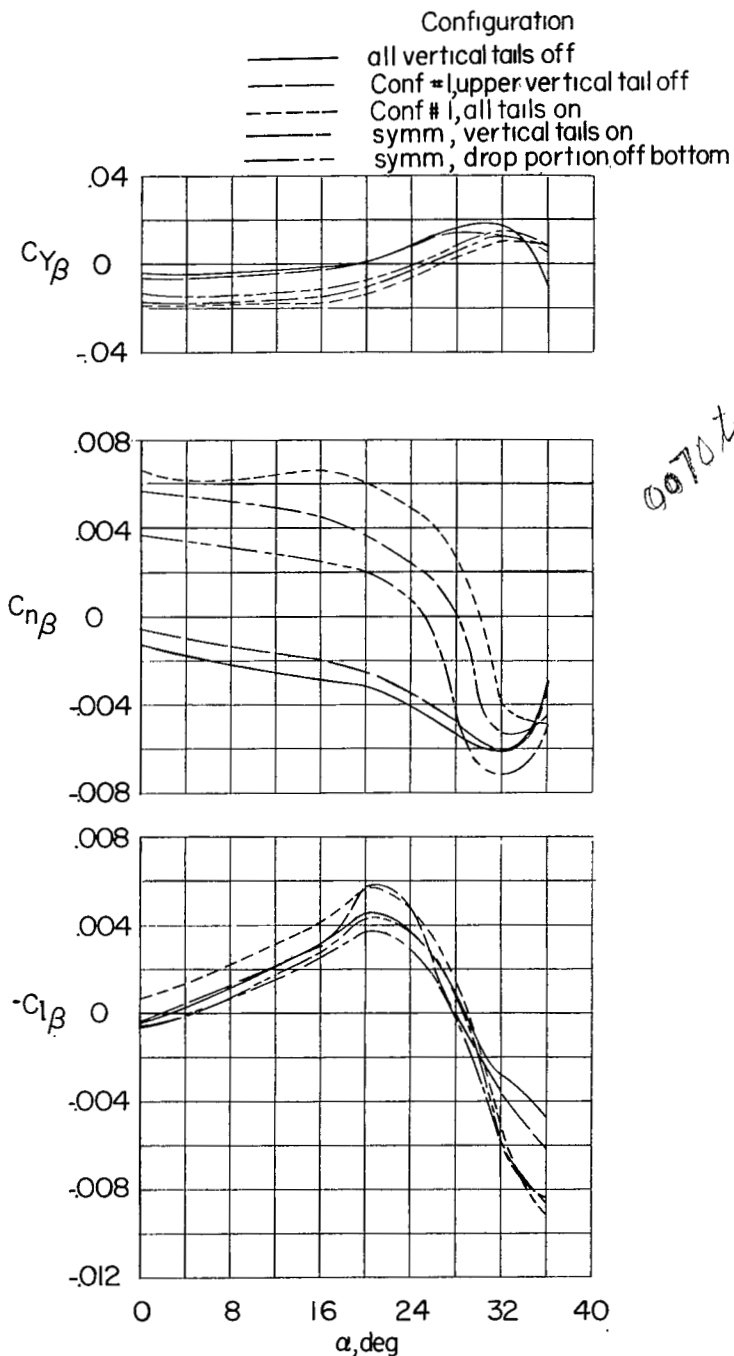


Figure 13.- Variation of static sideslip derivatives with angle of attack for two different tail configurations tested.  $\beta = \pm 5^\circ$ ;  $\delta_t = 0^\circ$ ;  $\delta_f = 0^\circ$ .

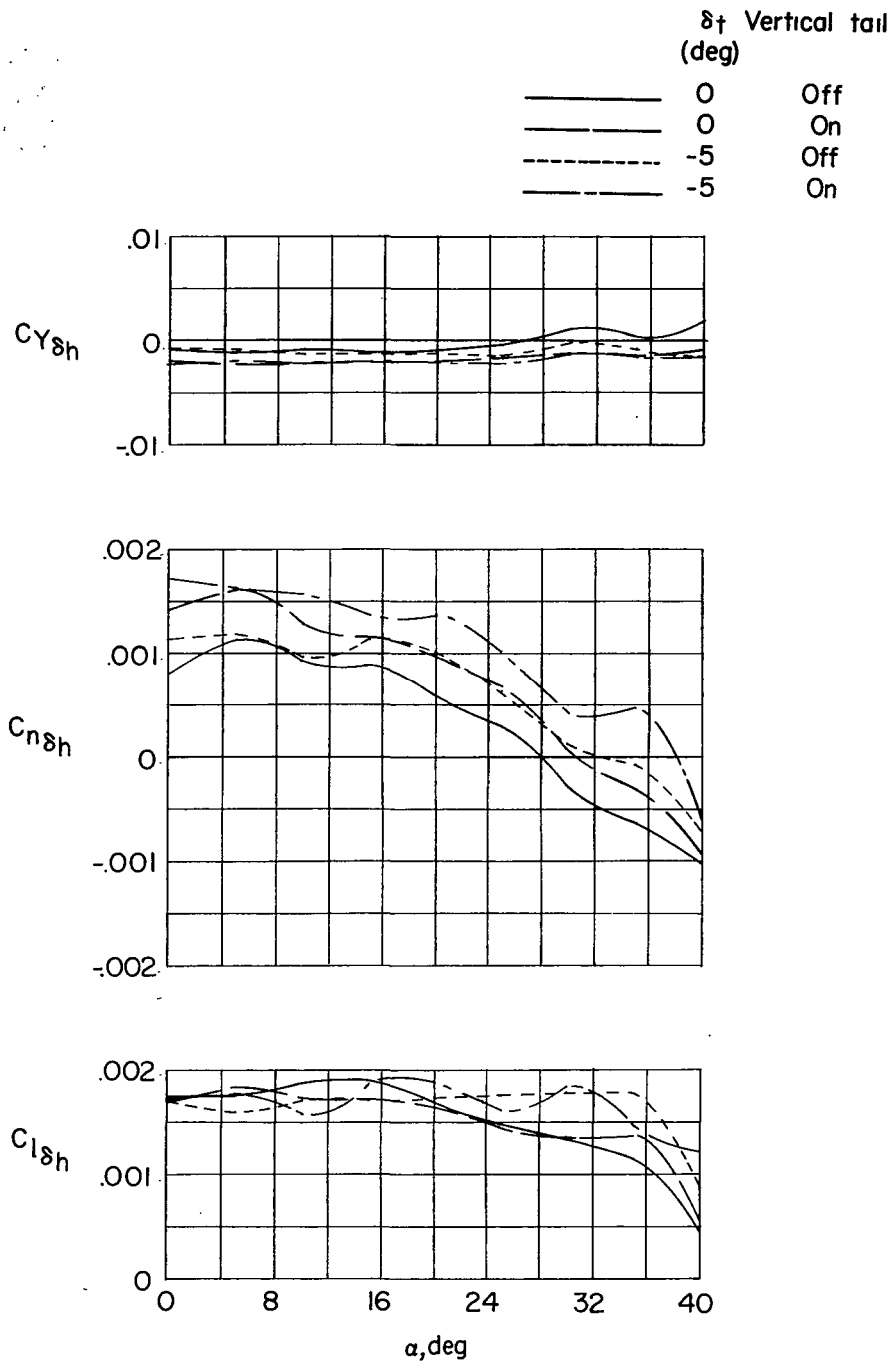


Figure 14.- Increments in lateral-force and moment coefficients produced by differential deflection of horizontal tail for model in clean configuration.  $\delta_F = 0^\circ$ .

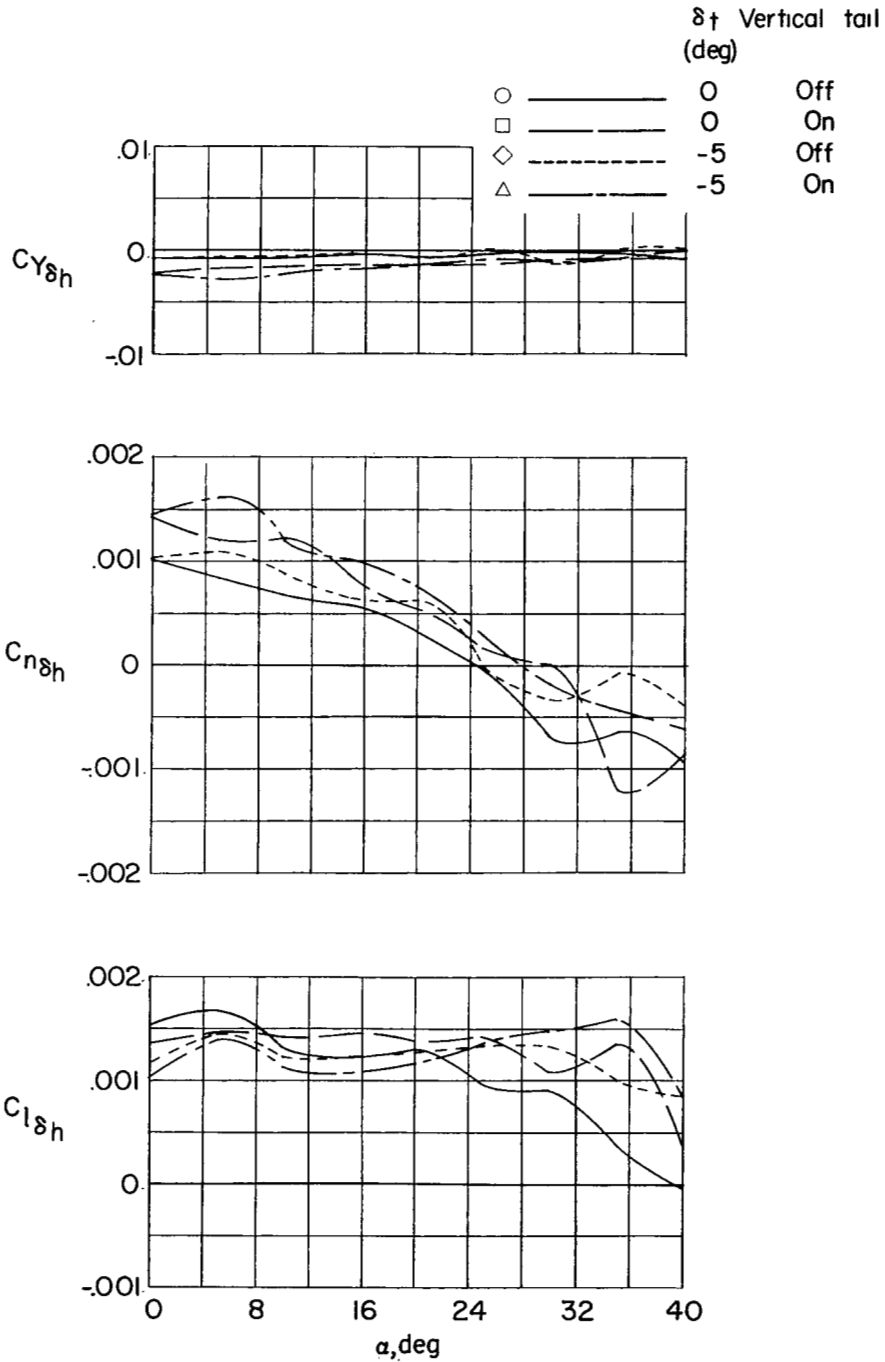


Figure 15.- Increments in lateral-force and moment coefficients produced by differential deflection of horizontal tail for model in landing configuration.  $\delta_f = 40^\circ$ .

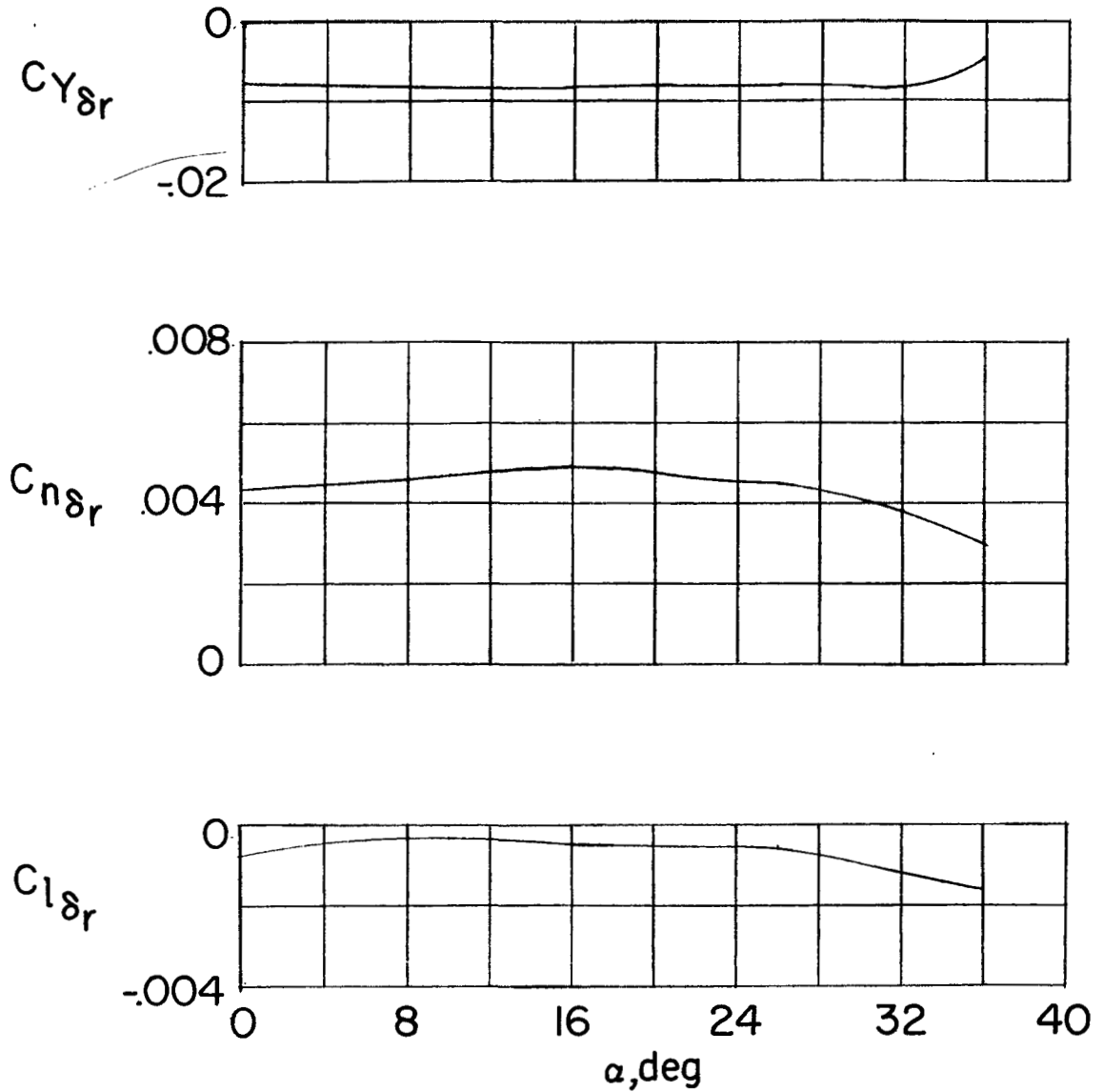


Figure 16.- Rudder effectiveness of model in clean configuration.  $\delta_t = 0^\circ$ ;  
 $\beta = 0^\circ$ .

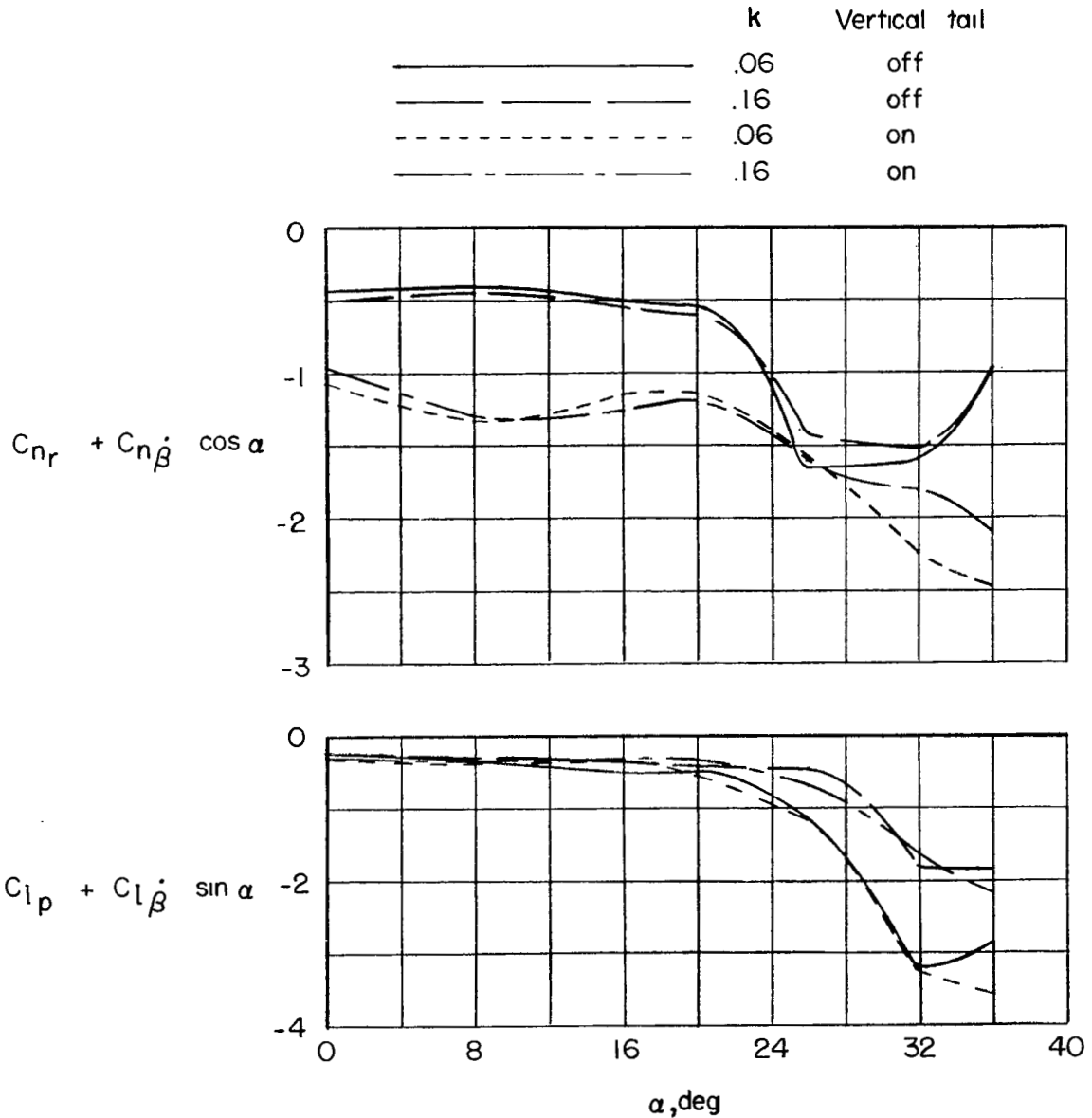


Figure 17.- Variation of  $C_{n_r} + C_{n\dot{\beta}} \cos \alpha$  and  $C_{l_p} + C_{l\dot{\beta}} \sin \alpha$  with frequency and angle of attack.  $\delta_f = 0^\circ$ ;  $\delta_t = 0^\circ$ .



A motion-picture film supplement, carrying the same classification as the report, is available on loan. Requests will be filled in the order received. You will be notified of the approximate date scheduled.

The film (16-mm., 10-min., B. & W., silent) deals with an investigation of the low-speed power-on stability and control characteristics of a 1/7-scale free-flying model similar to the North American X-15 airplane. The model was flown over an angle-of-attack range from 8° to 30° in the clean and the landing configurations and only relatively low-altitude conditions were simulated.

NOTE: It will expedite the handling of requests for this classified film if application for the loan is made by the individual to whom this copy of the report was issued. In line with established policy, classified material is sent only to previously designated individuals. Your cooperation in this regard will be appreciated.



CUT

-----

Date \_\_\_\_\_

Please send, on loan, copy of film supplement to RM L57D

---

Name of organization \_\_\_\_\_

---

Street number \_\_\_\_\_

---

City and State \_\_\_\_\_

Attention:\* Mr. \_\_\_\_\_

Title \_\_\_\_\_

\*To whom copy No. \_\_\_ of the RM was issued

Place  
stamp  
here

Chief, Division of Research Information  
National Advisory Committee for Aeronautics  
1512 H Street, N. W.  
Washington 25, D. C.

NASA Technical Library



3 1176 01437 9086

~~CONFIDENTIAL~~